

# Simulation of Multimodal Optical and Acoustic Communications in Underwater Networks

Filippo Campagnaro<sup>§</sup>, Federico Favaro<sup>§</sup>, Federico Guerra<sup>§</sup>,  
Violeta Sanjuan Calzado<sup>\*</sup>, Michele Zorzi<sup>§</sup>, Paolo Casari<sup>‡</sup>

<sup>§</sup>Department of Information Engineering, University of Padova, via Gradenigo 6/B, 35131 Padova, Italy

<sup>\*</sup>NATO STO Centre for Maritime Research and Experimentation, viale San Bartolomeo 400, La Spezia, Italy

<sup>‡</sup>IMDEA Networks Institute, Madrid, Spain

<sup>§</sup>{campagn1,favarofe,fguerra,zorzi}@dei.unipd.it

<sup>\*</sup>Violeta.Sanjuan@cmre.nato.int

<sup>‡</sup>paolo.casari@imdea.org

**Abstract**—In this paper, we consider data muling over a network of fixed sensors by employing a mobile Autonomous Underwater Vehicle (AUV). We approach the problem using both acoustic and optical communications together in a multi-modal hybrid network: the most appropriate physical layer is chosen according to the quality of the transmissions that take place over time. We consider three distinct cases of water type: clear, coastal and turbid water, in order to test the system behavior under different conditions. The ambient light noise is realistically reproduced via the Hydrolight software and taken into account, due to its important contribution to the optical SNR in shallow waters. Finally, we simulate the performance of the system using the DESERT Underwater framework during missions of interest in different channel conditions and network depth. Our results show the effectiveness of a multi-modal underwater network in the cases of clear and coastal waters.

**Index Terms**—Underwater acoustic networks, underwater optical networks, multi-modal underwater communications, ns2/NS-Miracle, Hydrolight.

## I. INTRODUCTION AND RELATED WORK

Underwater assets may be required to exchange information in order to accomplish a common task or mission. Acoustic communication systems are typically employed for underwater data transfer, as acoustic transmission and signal processing techniques have been developed for considerable time now, and have reached a remarkable level of maturity [1]–[3].

However, the missions that underwater networks of autonomous static and mobile assets may be required to carry out are diverse in nature, and may embrace periodic low-rate telemetry as well as fast, event-based data transfers, up to intense two-way point-to-point communications intended to, e.g., control Remotely Operated Vehicles (ROVs) [4] without the use of umbilical cables. As a consequence, today there is a growing interest in communicating through mediums other than the acoustic channel, by means of optical [5]–[7] or radio-frequency [8], [9] hardware. In this context, it is of great interest to simulate the behavior of underwater networks where nodes may carry out multi-modal communications via different kinds of communication technologies. This may involve not only optical, acoustic and RF communications, but also different implementations of either technology, e.g., multiple

acoustic modems working at different carrier frequencies, e.g., [2], [10].

An interesting problem that arises in this scenario is how the nodes should switch among different communication technologies, depending on the scenario, the requirements of the application, the environmental conditions or a combination of these factors. This issue is central to the optimization of the network performance, and may involve several layers of the protocol stack, such as the Medium Access Control (MAC), data-link, and routing layers. Some MAC solutions for acoustic networks exist, that manage communications across different bands in order to counter exogenous noise [11]. Extending MAC design to embrace multi-modal underwater communications complicates the setup, but still remains a very interesting task.

Before deploying any real technology, preliminary simulations are required to make sure that the devised solutions work as expected. In turn, this calls for a simulation framework able to support the implementation of such solutions.

Underwater optical communications have already been addressed in the literature. In [12], the authors provide a proof-of-concept for the use of Orthogonal Frequency-Division Multiplexing (OFDM) in underwater optical communications, giving a possible implementation of the PHY layer. In [13], the authors demonstrate the capabilities of underwater optical links, showing the possibilities to transmit also a video for real-time control. Also the feasibility of hybrid underwater networks has already been inspected. In [14] the authors describe a system where both acoustic and optical links are used. The downlink communication system, from the ship or base station to Autonomous Underwater Vehicles (AUVs), is a wide-angle low-bandwidth acoustic link, whereas uplink connections are high-bandwidth, highly-directional optical links. In [15] the authors present a multi-level Q-learning-based routing protocol for hybrid acoustic/optical communication. The work in [16] investigates optimal trajectory planning decisions for multiple AUVs in the presence of constraints on energy, data storage and retrieval requirements. Optical communications are exploited to retrieve data from sensors. Similarly, in [17] the

authors consider the value of the information retrieved by an AUV from a network of fixed underwater sensors, and propose a greedy path computation algorithm that approaches the maximum value obtained by solving an integer linear program.

In this paper, we present a new simulation tool for multi-modal underwater communications in networks of static and mobile nodes. We extend our ns2-based framework DESERT Underwater [18] to also model underwater optical links and provide additional modules to automatically manage the switch between the acoustic and the optical physical layers. The switch strategy is configurable by the user. We employ our simulator to test a scenario akin to [16], where an AUV moves to retrieve data from a number of bottom nodes. Our results prove that our optical/acoustic switch strategy (based on the perceived power over either link) is effective, and demonstrate the effect of different environmental parameters on the quality of the communication processes.

Compared to the current literature on underwater optical communications, we make one step further by employing Hydrolight [19], a state-of-the-art radiative transfer model that calculates the light propagation by taking into account the complexity of the real environment. Hydrolight solves the radiative transfer equation for multiple orders of scattering in a volume of water by including complex boundary conditions, sea surface roughness, bottom reflectance and inelastic processes for a given solar elevation angle. The radiant power is calculated and quad-averaged for the full anisotropic radiant distribution. The inputs of the model are the inherent optical properties of the water, absorption, scattering, attenuation and volume scattering function; the model outputs are the radiant power and its derived quantities. Hydrolight allows us to recreate real scenarios and to evaluate the background ambient light and thereby characterize the performance of the optical system for various realistic oceanographic conditions.

## II. DESERT v2 FRAMEWORK AND MULTI-PHY EXTENSIONS

All simulation results presented in this paper were obtained using a set of C/C++ libraries to simulate multimodal communications in underwater networks, which have been implemented as part of the DESERT Underwater v2 software [18] released as open-source at [20]. Several components have been added to support multi-modal communications; the functions of these modules can be broadly categorized as follows:

- support for multiple physical layers on the same node,
- transmission, propagation and reception models for underwater optical signals,
- control of physical layer use and automatic switch among them based on user-defined algorithms.

In particular, the protocol stack implemented in each simulated node is organized as follows:

- CBR (Constant Bit Rate application layer)
- ALOHA – TRIGGER
- MULTI – STACK – CONTROLLER

- ACOUSTIC PHY LAYER
- OPTICAL PHY LAYER

The CBR application layer is configured to continuously generate data packets of 125 bytes at a fixed rate, in such a way that the queues of the nodes are never empty. We adapted the ALOHA – TRIGGER MAC protocol from [21]. This protocol has two primary operational modes: AUV and NODE. In the former, it periodically sends a TRIGGER packet and then listens to incoming data packets from the other peers in NODE mode for a fixed amount of time before a new cycle is started. In NODE mode the protocol waits for the TRIGGER packet: after its reception, it behaves according to the normal Aloha protocol, sending its data packets in a random access fashion. The MULTI – STACK – CONTROLLER is the module that controls which PHY layer is going to be used for the next ALOHA – TRIGGER’s transmission round, forwarding the packets coming from upper layers accordingly.

The stack also includes the UDP, IP, and MLL modules, which are standardly used in most DESERT simulation runs, and are described in greater detail in [18].

The PHY layer switch policy is based upon the average power collected during a complete trigger cycle, and therefore avoids any additional signaling. During a trigger period, only the selected PHY can be used to transmit, in order to limit the power consumption. The PHY layer switch algorithm is implemented as follows. We calculate the transmission range  $d$  corresponding to an optical Signal-to-Noise Ratio (SNR) of 20 dB, and define  $\theta_{opt}$  as the received *optical* power at a distance  $d+0.5$  m. We then define  $\theta_{ac}$  as the received *acoustic* power at a distance  $d-0.5$  m. The hysteresis of 0.5 m provides a sufficient margin to avoid continuous switching between acoustic and optical communications. The switch from the acoustic to the optical PHY is operated after the reception of packet  $k$  whenever  $\bar{P}_{r,ac}(k) > \theta_{ac}$ , where  $\bar{P}_{r,ac}(k)$  is the average receiver-side acoustic power after the reception of packet  $k$ : this value is updated at every received packet  $i$  according to the relationship

$$\bar{P}_{r,ac}(i) = \alpha P_{r,ac}(i) + (1 - \alpha)\bar{P}_{r,ac}(i - 1), \quad (1)$$

where  $P_{r,ac}(i)$  is the received power of packet  $i$ , and it is understood that  $\bar{P}_{r,ac}(0) = 0$  and  $\bar{P}_{r,ac}(1) = P_{r,ac}(1)$ . The switch from the optical to the acoustic physical layer is similarly triggered after the reception of packet  $\ell$  as  $\bar{P}_{r,opt}(\ell) < \theta_{opt}$ , where  $\bar{P}_{r,opt}(\ell)$  is the average receiver-side optical power after the reception of packet  $\ell$ , and is filtered over time analogously to (1).

The MULTI – STACK – CONTROLLER on the AUV node decides the physical layer once the ALOHA – TRIGGER sends its TRIGGER packet. The optical noise of the sun light is taken into account via offline runs of Hydrolight [19]. The Hydrolight output is imported into DESERT in the form of a lookup table, containing the ambient light noise as a function of the position in the water column. The receiver model determines whether an optical signal has been correctly received based on the calculated SNR: the optical transmission model is described in [7], while the Hydrolight noise power is added to the device

TABLE I  
ABSORPTION, SCATTERING AND ATTENUATION COEFFICIENTS OF  
VARIOUS WATER TYPES.

Water type	$a$ [ $\text{m}^{-1}$ ]	$b$ [ $\text{m}^{-1}$ ]	$c$ [ $\text{m}^{-1}$ ]
clear ocean	0.1	0.05	0.15
coastal ocean	0.2	0.2	0.4
turbid harbor	0.5	1.69	2.19

noise in the SNR calculation. These features will be released in the next version of the DESERT Underwater framework [20].

### III. SIMULATION SCENARIO AND SYSTEM CONFIGURATION

#### A. Scenario

We set up a simulation scenario with 8 nodes arranged in a  $4 \times 2$  rectangular grid topology, with nearest neighbors 100 m apart. The environmental conditions include no wind, no clouds and a shipping factor of 0. We set  $\alpha = 0.5$  for the IIR filter in (1). The network is deployed in the Mediterranean sea ( $44.509^\circ\text{N}$ ,  $13.5^\circ\text{E}$ ). Latitude and longitude are fixed, while we have considered many combinations of different depths and water types (Table I), in order to evaluate and compare the network performance in several environmental conditions.

The AUV patrols the network following a clockwise way-point trajectory at a speed of 2 knots. Each way-point is placed in correspondence of each node, located at the same latitude and longitude, but 1.5 m above the nodes. The AUV can stop at each way-point for a time  $t_{stop}$ . Our goal is to find the minimum  $t_{stop}$  that enables a successful technology switch in the proximity of all the nodes. We observe the network behavior during one complete AUV lap for several combinations of  $t_{stop}$ , network depth and water type. The speed of sound under water is assumed to be constant and equal to 1500 m/s, while the speed of light underwater is set to  $\approx 2.25 \cdot 10^8$  m/s. We simulate the behavior of the Evologics S2CR 18/34 acoustic modem [10] for acoustic communications; this modem works at a carrier frequency of 26 kHz and provides a bandwidth of 16 kHz, a nominal maximum transmission rate of 13.9 kbps (as reported in the modem data sheet [10]), a maximum transmission power of 80 W and nominal SNR of 10 dB. The acoustic bit rate is set to 10 kbps, with a source level of 158 dB re  $\mu\text{Pa}^2$  at 1 m from the source. The optical transmission model is described in [7], supposing to use an optical wavelength  $\lambda = 514$  nm. The receiver uses a Si PIN Hamamatsu S5971 high-speed photodiode [22], with transmitting area  $A_r = 1.1$  mm<sup>2</sup>, sensitivity  $S = 0.26$  A/W, maximum dark current  $I_p = 1$  nA, shunt resistance  $R = 1.43 \cdot 10^9$   $\Omega$  and an optical bandwidth of 100 kHz as in [7]. The optical transmitter has beam divergence angle  $\theta = 0.5$  rad,  $A_t = 10$  mm<sup>2</sup>, a transmission rate of 1 Mpbs and a transmission power of 100 W.<sup>1</sup> In addition, we force perfect alignment between transmitter and receiver.

<sup>1</sup>High-power LEDs with transmitting power of 100 W are available off-the-shelf [23]; in addition, Amalux [24] provides an underwater optical modem able to transmit at a power of up to 100 W.

TABLE II  
 $E_0$  AT A DEPTH OF 30 M, IN A 40 M WATER COLUMN FOR DIFFERENT  
WATER CONDITIONS. IN AIR,  $E_0 \approx 2.06$  W/m<sup>2</sup>.

$c$ [ $\text{m}^{-1}$ ]	$a$ [ $\text{m}^{-1}$ ]	$b$ [ $\text{m}^{-1}$ ]	$E_0$ [W/m <sup>2</sup> ]
0.15	0.15	0.00	$1.25 \cdot 10^{-2}$
0.15	0.00	0.15	3.3879
0.15	0.10	0.05	$5.66 \cdot 10^{-2}$
0.40	0.40	0.00	$4.80 \cdot 10^{-6}$
0.40	0.00	0.40	3.69
0.40	0.20	0.20	$1.41 \cdot 10^{-3}$
2.19	2.19	0.00	$5.84 \cdot 10^{-30}$
2.19	0.00	2.19	3.2219
2.19	0.50	1.69	$6.11 \cdot 10^{-10}$

This approximation can be justified by considering an omnidirectional transmitter, such as [25], [26], or assuming that the combination of both the AUV slow speed and  $t_{stop}$  provides enough time for a correct alignment. The optical SNR threshold for a correct packet reception is set to 20 dB.

#### B. Ambient light noise and attenuation coefficient

Due to the system design, the physical layer choice is strictly correlated to the optical transmission range available. This value depends on both the contribution of the attenuation coefficient and the ambient noise caused by the solar irradiance  $E_0$ . For this reason, by employing different combinations of  $c$  and  $E_0$  it is possible to achieve the same optical transmission range. For instance, in our system a transmission range around 10 m is achieved either with an attenuation coefficient  $c = 0.15$  m<sup>-1</sup> and a sunlight noise  $E_0 = 0.1$  W/m<sup>2</sup>, or with  $c = 0.4$  m<sup>-1</sup> and  $E_0 = 0.01$  W/m<sup>2</sup>. The ambient light propagation depends on the water type, water column depth and solar zenith angle. We assume to transmit in a water column of 100 m during sunrise or sunset, when the solar angle is about 0°. However, as explained in Section III-C, similar ambient light powers are obtained either by setting a different solar angle or in a shallower water column of 40 m. A different behavior is found in very shallow water, e.g., in a water column of maximum depth 10 m, where the bottom reflection causes a higher level of ambient light noise. Although the propagation of the transmitting signal depends on the total attenuation coefficient  $c$ , from the Hydrolight runs we obtain that the main cause of solar light attenuation is the absorption coefficient. This behavior is reported in Table II. Although the study of the attenuation coefficient by varying  $a$  and  $b$  is an interesting topic, in our simulations we employ the partitions described in Table I, because they match well with some real cases.

In order to compare the network performance versus the ambient light noise in each water type, we simulate the system by varying  $E_0$  from 0 to the value it assumes around a depth of 5 m. The ambient light noise power  $N_A$  is obtained as

$$N_A = (S \cdot E_0 \cdot A_r)^2 \quad (2)$$

$N_A$  is then added to the device noise in the SNR calculation. As shown in Fig. 1, the sunlight noise becomes the main factor

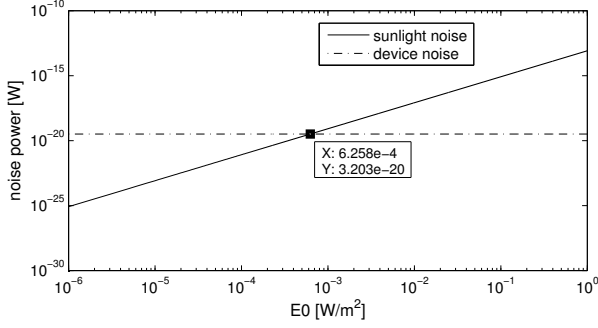


Figure 1. Sunlight noise power vs.  $E_0$ .

in the total noise power when  $E_0 > 6.26 \cdot 10^{-4} \text{ W/m}^2$ . From the point of view of network simulations, the system behavior is very similar to the case of no ambient light noise whenever  $E_0 < 10^{-3} \text{ W/m}^2$ .

### C. Optical and acoustic threshold

In Table III we report the optical and the acoustic thresholds obtained as explained in Section II, for different values of the ambient light noise and the attenuation coefficient. In addition, we report the corresponding optical transmission range and the network deployment depth. The latter refers to a water column of 100 m with a solar angle of  $0^\circ$ , however, the same results were obtained in a water column of 40 m. Although the bottom reflections cause a higher ambient light noise in a water column of 10 m, we observed that setting  $c = 0.4 \text{ m}^{-1}$  or  $c = 2.19 \text{ m}^{-1}$  leads to the same results. Conversely, when the attenuation coefficient is  $0.15 \text{ m}^{-1}$ , we obtain a higher ambient light noise (for example  $E_0 = 0.9 \text{ W/m}^2$  at 8.5 m). Very similar values were obtained also in the case of different sunlight inclinations: for instance, with a solar zenith angle of  $22^\circ$  (corresponding to the summer solstice zenith angle in La Spezia, Italy) and a water column of depth 100 m, if the system is placed 1 meter closer to the surface than in the previous case, the same ambient light noise conditions are obtained.

By employing different partitions of the attenuation coefficient  $c$ , the same values of  $E_0$  are retrieved at different depths. On one hand, by increasing the scattering coefficient  $b$ , the same sunlight noise has been found in deeper water. On the other hand, with a higher attenuation coefficient  $a$ , the same ambient light noise power has been retrieved closer to the surface. In the case of  $c = 0.15 \text{ m}^{-1}$ , a value of  $E_0$  around  $0.1 \text{ W/m}^2$  has been retrieved either at a depth of 16 m if  $a = 0.15 \text{ m}^{-1}$ , 24 m if  $a = 0.1 \text{ m}^{-1}$ , 32 m if  $a = 0.075 \text{ m}^{-1}$ , or at a depth of more than 100 m if  $a = 0 \text{ m}^{-1}$ .

## IV. RESULTS AND PERFORMANCE COMPARISON

In our simulations, we focused on the system throughput and the minimum value of  $t_{stop}$  required to ensure a correct switch between acoustic and optical physical layer. The average system throughput is calculated over 10-s time intervals and plotted in the location of the AUV at the end of each

TABLE III  
OPTICAL AND ACOUSTIC THRESHOLDS WITH HYSTERESIS OF 0.5 M.

$c \text{ [m}^{-1}\text{]}$	$E_0 \text{ [W/m}^2\text{]}$	optTh [W]	acTh [dB]	range [m]	depth [m]
0.15	0	$6.20 \cdot 10^{-9}$	135.7	30.12	100.0
0.15	0.001	$1.16 \cdot 10^{-8}$	136.6	27.25	69.5
0.15	0.01	$9.77 \cdot 10^{-8}$	139.1	18.25	48.5
0.15	0.1	$9.23 \cdot 10^{-7}$	143.0	10.45	27.5
0.15	0.5	$4.46 \cdot 10^{-6}$	146.5	6.32	12.5
0.15	0.9	$8.07 \cdot 10^{-6}$	148.0	5.15	6.5
0.4	0	$4.83 \cdot 10^{-9}$	140.5	15	100.0
0.4	0.001	$9.94 \cdot 10^{-9}$	141.1	13.65	33.5
0.4	0.01	$8.25 \cdot 10^{-8}$	143.3	9.91	23.5
0.4	0.1	$7.87 \cdot 10^{-7}$	146.5	6.35	13.5
0.4	0.5	$3.64 \cdot 10^{-6}$	149.3	4.31	6.5
2.19	0	$1.69 \cdot 10^{-9}$	149.9	3.95	100.0
2.19	0.001	$3.74 \cdot 10^{-9}$	150.5	3.65	12.5
2.19	0.01	$2.88 \cdot 10^{-8}$	152.3	2.91	9.5
2.19	0.1	$2.45 \cdot 10^{-7}$	154.7	2.15	5.5

TABLE IV  
SYSTEM PERFORMANCE.

$c \text{ [m}^{-1}\text{]}$	$E_0 \text{ [W/m}^2\text{]}$	range [m]	$t_{stop}$ [s]	thr [bps]	opt %
0.15	0	30.12	0	$3.57 \cdot 10^5$	53.80
0.15	0.001	27.25	0	$3.03 \cdot 10^5$	46.80
0.15	0.01	18.25	0	$1.77 \cdot 10^5$	29.78
0.15	0.1	10.45	0	$0.80 \cdot 10^5$	17.09
0.15	0.5	6.32	0.74	$0.31 \cdot 10^5$	9.76
0.15	0.9	5.15	2.55	$0.24 \cdot 10^5$	4.88
0.4	0	15	0	$1.61 \cdot 10^5$	27.50
0.4	0.001	13.65	0	$1.38 \cdot 10^5$	24.37
0.4	0.01	9.91	0	$0.82 \cdot 10^5$	18.12
0.4	0.1	6.35	0	$0.34 \cdot 10^5$	9.38
0.4	0.5	4.31	2.60	$0.23 \cdot 10^5$	4.88
2.19	0	3.95	3.50	$0.33 \cdot 10^5$	10.37
2.19	0.001	3.65	4.05	$0.30 \cdot 10^5$	8.54
2.19	0.01	2.91	5.90	$0.30 \cdot 10^5$	8.93
2.19	0.1	2.15	7.80	$0.16 \cdot 10^5$	6.98

10-s period. As expected, the optical communications range plays the most important role in determining the network behavior: the longer the range, the bigger the amount of data transmitted and the smaller  $t_{stop}$ . Another interesting metric is the percentage ratio of optical trigger periods over the total number of trigger periods, which is used to estimate the usage level for high-rate optical communications. We report the resulting performance in Table IV.

For those combinations of  $E_0$  and  $c$  that lead to an optical range of at least 6.35 m, we can set  $t_{stop} = 0$ , as a switch to optical communications will always take place and be successful. Instead, when range is shorter, if the AUV waits in each way-point less than the value of  $t_{stop}$  reported in Table IV, the switch to optical communications does not take place correctly. A comparison of the system behavior for  $t_{stop} = 0$  and different cases of  $E_0$  is plotted in Fig. 2 ( $c = 0.15 \text{ m}^{-1}$ ), Fig. 3 ( $c = 0.4 \text{ m}^{-1}$ ) and Fig. 4 ( $c = 2.19 \text{ m}^{-1}$ ). In these figures the throughput of the system is plotted versus the simulation time, when the AUV passes over the first three waypoints of the path.

A correct switch occurs when the throughput increases in

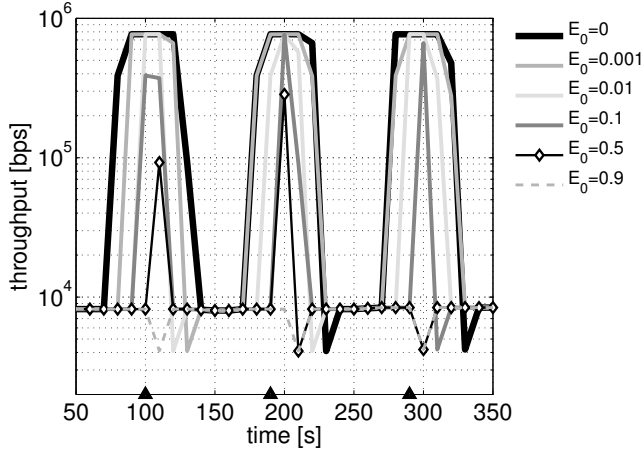


Figure 2. Throughput comparison versus simulation time, for the first three waypoints path, for different cases of  $E_0$ ,  $c = 0.15m^{-1}$  and  $t_{stop} = 0 s$ .

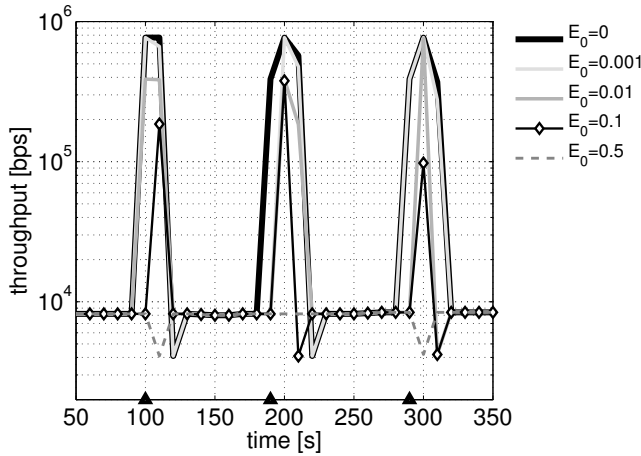


Figure 3. Throughput comparison versus simulation time, for the first three waypoints path, for different cases of  $E_0$ ,  $c = 0.4m^{-1}$  and  $t_{stop} = 0 s$ .

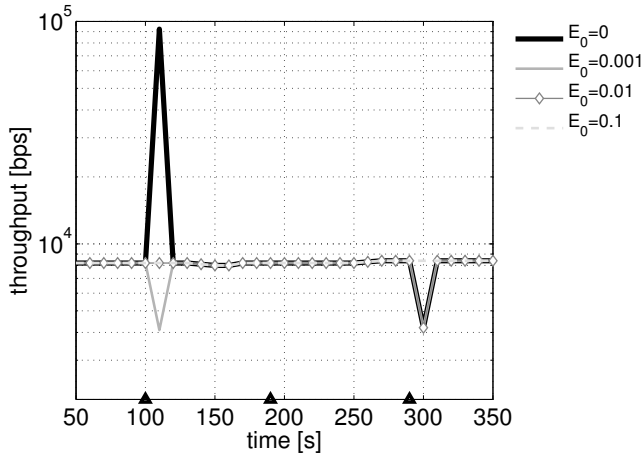


Figure 4. Throughput comparison versus simulation time, for the first three waypoints path, for different cases of  $E_0$ ,  $c = 2.19m^{-1}$  and  $t_{stop} = 0 s$ .

the proximity of a way-point (represented with a triangle). However, the throughput drops if the system tries to transmit when the optical modem is out of range. For  $t_{stop} = 0 s$ , the correct switch occurs in every way-point in case of both clear and coastal water with  $E_0 \leq 0.1 W/m^2$ . Instead, with  $E_0 \geq 0.5 W/m^2$ , it may happen that the switch happens too

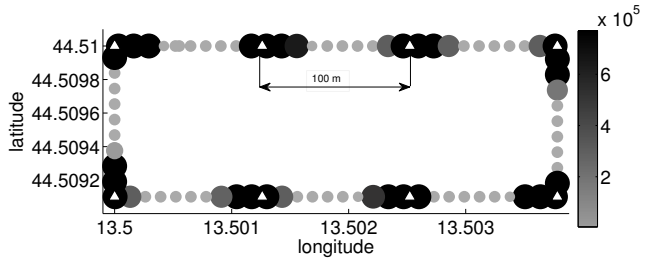
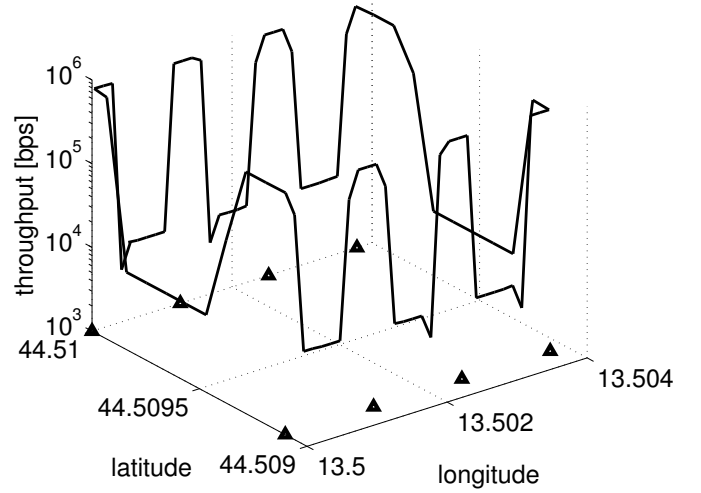


Figure 5. Throughput versus position of one clockwise lap.  $E_0 = 0.001 W/m^2$ ,  $c = 0.15 m^{-1}$  and  $t_{stop} = 0 s$ .

late, when the optical modems are out of range. In turbid waters, this anomalous behavior occurs more frequently; in addition, the switch does not occur in some cases because the available average power measurement does not exceed the acoustic threshold. This wrong behavior is due to the trigger delay caused by the combination of both trigger time, hysteresis and AUV speed. However, this problem can be solved by employing a higher  $t_{stop}$ .

The results have the same trend in the cases of similar optical transmission range and the same  $t_{stop}$ . Four examples of throughput versus position are reported, both in 3D plots and in 2D projections. In the latter, the performance metric is represented using gray-scale points, with a circle area proportional to the throughput values.<sup>2</sup> The way-points are represented by triangles.

Fig. 5 reports the throughput of the system placed in clear ocean water at a depth of 69.5 m, where  $E_0 = 0.001 W/m^2$ . The achievable optical range is 27.25 m,  $t_{stop} = 0$ , and the percentage of optical triggers is about 47%. The environmental conditions are very advantageous for the optical transmission, indeed, many consecutive optical triggers are successfully sent to each node (8.75, on average), thus, a big amount of data can be retrieved (the average throughput is 303 kbps). In addition, just 4 out-of-range optical triggers are sent during

<sup>2</sup>E.g., a small light grey circle represents a throughput of a few kbps, whereas a thick black circle represents a throughput of about 0.8 Mbps.

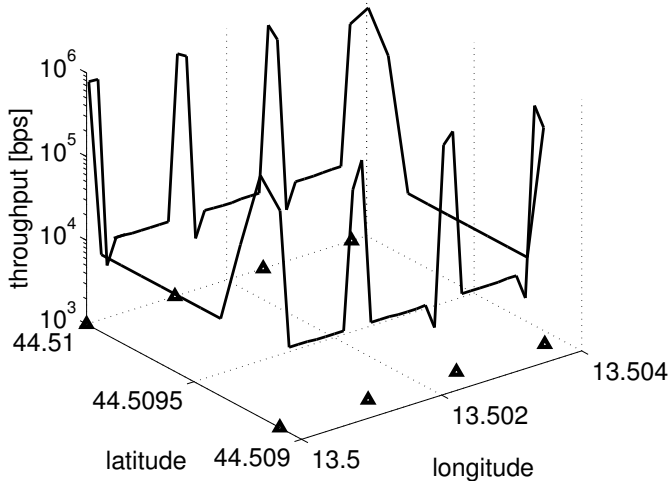


Figure 6. Throughput versus position of one clockwise lap.  $E_0 = 0.001 \text{ W/m}^2$ ,  $c = 0.4 \text{ m}^{-1}$  and  $t_{stop} = 0 \text{ s}$ .

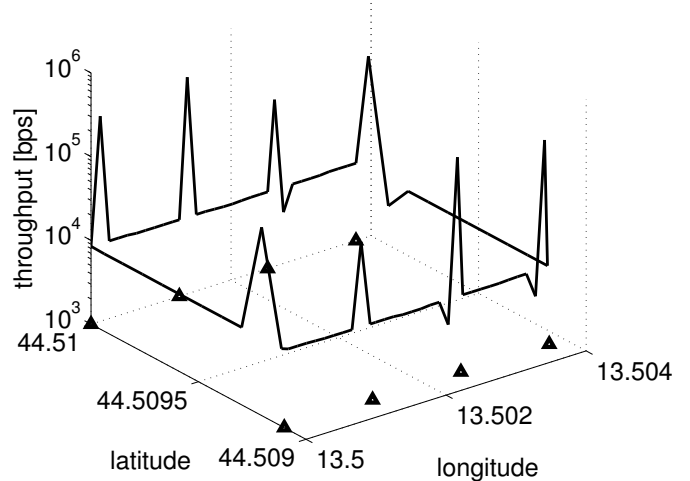


Figure 7. Throughput versus position of one clockwise lap.  $E_0 = 0.001 \text{ W/m}^2$ ,  $c = 2.19 \text{ m}^{-1}$  and  $t_{stop} = 4.05 \text{ s}$ .

the entire lap (5.4% of the total number of optical triggers), without causing significant performance losses compared to the benefits provided. Very similar results have been found in deeper waters, where the ambient light noise is negligible and the optical communications range is about 30 m.

Fig. 6 reports the throughput of the system placed in coastal ocean water at depth 33.5 m, where  $E_0 = 0.001 \text{ W/m}^2$ . In this case the optical range is 13.65 m,  $t_{stop} = 0$  and the percentage of optical triggers is around 25%. With these conditions, more consecutive optical triggers are successfully sent to each node (4.25, on average), thus, a big amount of data can be retrieved (the average throughput is 138 kbps). In addition, just 5 out-of-range optical triggers are sent during the entire lap (12.8% of all optical triggers), again without causing significant performance loss. Similar results have been found in deeper water, where the ambient light noise is negligible and the optical communications range is about 15 m, and in the case of clear water at a depth of 48.5 m.

Finally, Fig. 7 reports the throughput of the system in turbid ocean waters at a depth of 12.5 m, where  $E_0 = 0.001 \text{ W/m}^2$ . In this case, the optical range is 3.65 m,  $t_{stop} = 4.05 \text{ s}$ , and the percentage of optical triggers is about 12.5%. With these disadvantageous conditions, only one optical trigger can be successfully sent in correspondence of each node (1.25, on average). Therefore, optical communications are employed only for a small period of time and the average throughput is 30 kbps. In addition, 4 out-of-range optical triggers are sent

during the entire lap, i.e., 28.6% of the total number of optical triggers, causing further performance losses. Similar results have been found in the other disadvantageous cases: both turbid water and clear and coastal water with  $E_0 \geq 0.5 \text{ W/m}^2$ , by employing the corresponding minimum  $t_{stop}$  to achieve the switch. When the optical range is less than 6.35 m,  $t_{stop}$  must be set to a value greater than 0. Using the minimum time to allow the switching to take place correctly, very similar results are obtained.

## V. CONCLUSIONS

In this paper we presented a multi-modal acoustic and optical underwater network, able to retrieve large amounts of data if the optical transmission range is longer than 9 m. By using the DESERT Underwater framework and by factoring in the sunlight noise predicted by Hydrolight runs, we compared the system performance under different water types and ambient light noise levels, in order to understand in which conditions multimodal communications provide significant benefits. The results show that a high throughput can be obtained in most cases in both clear and coastal sea water. However, also for worst-case communication conditions, a high throughput can be achieved by having the AUV stop for a sufficiently long time in the proximity of each node, at the cost of increasing the total time required to complete a lap.

## ACKNOWLEDGMENTS

This work has been supported in part by the US Office of Naval Research under Grant no. N62909-14-1-N127.

## REFERENCES

- [1] M. Chitre, S. Shahabudeen, and M. Stojanovic, "Underwater acoustic communications and networking: Recent advances and future challenges," *Marine Tech. Soc. Journal*, vol. 42, no. 1, pp. 103–116, spring 2008.
- [2] P.-P. Beaujean, J. Spruance, E. A. Carlson, and D. Kriel, "HERMES - A high-speed acoustic modem for real-time transmission of uncompressed image and status transmission in port environment and very shallow water," in *Proc. MTS/IEEE Oceans*, Québec City, Canada, Sep. 2008.
- [3] E. Gallimore, J. Partan, I. Vaughn, S. Singh, J. Shusta, and L. Freitag, "The WHOI micromodem-2: A scalable system for acoustic communications and networking," in *Proc. MTS/IEEE Oceans*, Seattle, WA, Sep. 2010.
- [4] F. Campagnaro, F. Favaro, P. Casari, and M. Zorzi, "On the feasibility of fully wireless remote control for underwater vehicles," in *Proc. Asilomar Conf. SS&C*, Pacific Grove, CA, Nov. 2014.
- [5] N. Farr, A. Bowen, J. Ware, C. Pontbriand, and M. Tivey, "An integrated, underwater optical/acoustic communications system," in *Proc. MTS/IEEE Oceans*, Sydney, Australia, May 2010.
- [6] Y. Ito, S. Haruyama, and M. Nakagawa, "Short-range underwater wireless communication using visible light LEDs," *WSEAS Trans. Commun.*, vol. 9, pp. 525–552, Sep. 2010.
- [7] D. Anguita, D. Brizzolara, G. Parodi, and Q. Hu, "Optical wireless underwater communication for AUV: Preliminary simulation and experimental results," in *Proc. IEEE/OES Oceans*, Santander, Spain, Jun. 2011.
- [8] X. Che, I. Wells, G. Dickers, P. Kear, and X. Gong, "Re-evaluation of RF electromagnetic communication in underwater sensor networks," *IEEE Commun. Mag.*, vol. 48, no. 12, pp. 143–151, Dec. 2010.
- [9] A. Palmeiro, M. Martín, I. Crowther, and M. Rhodes, "Underwater radio frequency communications," in *Proc. IEEE/OES Oceans*, Santander, Spain, Jun. 2011.
- [10] "Evologics underwater SC2R acoustic modem series," accessed: Oct. 2014. [Online]. Available: <http://www.evologics.de/en/products/acoustics/index.html>
- [11] L. Pescosolido, C. Petrioli, and L. Picari, "A multi-band noise-aware MAC protocol for underwater acoustic sensor networks," in *Proc. IEEE WiMob*, Lyon, France, Oct. 2013.
- [12] P. Minev, C. Tsimenidis, and B. Sharif, "Short-range optical OFDM," in *Proc. IEEE/OES OCEANS*, Yeosu, Korea, May 2012.
- [13] N. Farr, A. Bowen, J. Ware, C. Pontbriand, and M. Tivey, "An integrated, underwater optical/acoustic communications system," in *Proc. IEEE/OES OCEANS*, Sydney, Australia, May 2010.
- [14] L. Johnson, R. Green, and M. Leeson, "Hybrid underwater optical/acoustic link design," in *Proc. ICTON*, Graz, Austria, Jul. 2014.
- [15] T. Hu and Y. Fei, "MURAO: A multi-level routing protocol for acoustic-optical hybrid underwater wireless sensor networks," in *Proc. IEEE SECON*, Seoul, Korea, Jun. 2012.
- [16] P. A. Forero, S. Lopic, C. Wakayama, and M. Zorzi, "Rollout algorithms for data storage- and energy-aware data retrieval using autonomous underwater vehicles," in *Proc. ACM WUWNet*, Rome, Italy, Nov. 2014.
- [17] S. Basagni, L. Bölöni, P. Gjanci, C. Petrioli, C. A. Phillips, and D. Turgut, "Maximizing the value of sensed information in underwater wireless sensor networks via an autonomous underwater vehicle," in *Proc. IEEE INFOCOM*, Toronto, Canada, Apr. 2014, pp. 988–996.
- [18] P. Casari *et al.*, "Open-source suites for the underwater networking community: WOSS and DESERT Underwater," *IEEE Network, special issue on "Open Source for Networking: Development and Experimentation"*, vol. 28, no. 5, pp. 38–46, Sep. 2014.
- [19] Sequoia Scientific, "Hydrolight radiative transfer numerical model," Last time accessed: Dec. 2014. [Online]. Available: <http://www.sequoiasci.com/product/hydrolight/>
- [20] "DESERT Underwater github repository." [Online]. Available: [https://github.com/uwsignet/DESERT\\_Underwater](https://github.com/uwsignet/DESERT_Underwater)
- [21] F. Favaro, P. Casari, F. Guerra, and M. Zorzi, "Data upload from a static underwater network to an AUV: Polling or random access?" in *Proc. MTS/IEEE Oceans*, Yeosu, Republic of Korea, May 2012.
- [22] "Si PIN photodiode S5971," accessed: March 2015. [Online]. Available: <http://www.hamamatsu.com/eu/en/product/category/3100/4001/4103/S5971/index.html>
- [23] "100 W blue high power LED," accessed: March 2015. [Online]. Available: [http://www.topledlight.com/100w-blue-high-power-led\\_p276.html](http://www.topledlight.com/100w-blue-high-power-led_p276.html)
- [24] "Ambalux 1013C1 high-bandwidth underwater transceiver," Accessed: Oct. 2014. [Online]. Available: [http://www.ambalux.com/gdresources/media/AMB\\_1013\\_Brochure.pdf](http://www.ambalux.com/gdresources/media/AMB_1013_Brochure.pdf)
- [25] G. Baiden and Y. Bissiri, "High bandwidth optical networking for underwater untethered telerobotic operation," in *Proc. MTS/IEEE Oceans*, Vancouver, Canada, Sep. 2007.
- [26] N. Farr, A. D. Chave, L. Freitag, J. Preisig, S. N. White, D. Yoerger, and F. Sonnichsen, "Optical modem technology for seafloor observatories," in *Proc. MTS/IEEE Oceans*, Boston, MA, Sep. 2006.